BEM Modeling of Inflow with Shear in Comparison with Advanced Model Results

F. Grasso

Published in: Wind Energy Journal,Wiley,
Vol.15, Issue 1, pp.63-81. DOI: 10.1002/we.493

ECN-W--11-015 FEBRUARY 2012

WIND ENERGY
Wind Energ. 2012; **15**:63–81
Published online 3 October 2011 in Wiley Online Library (wileyonlinelibrary.com). DOI: 10.1002/we.493

SPECIAL ISSUE PAPER

Blade element momentum modeling of inflow with shear in comparison with advanced model results

H. Aa. Madsen[1], V. Riziotis[2], F. Zahle[1], M. O. L. Hansen[3], H. Snel[4], F. Grasso[4], T. J. Larsen[1], E. Politis[5] and F. Rasmussen[1]

[1]Wind Energy Division, Risø DTU, Building 118, DK-4000 Roskilde, Denmark
[2]NTUA, 9 Heroon Polytechniou str.15780, Athens, Greece
[3]DTU Mechanics, Nils Koppels Alle build. 403, DK-2800 Lyngby, Denmark
[4]ECN Wind Energy, P.O. Box 1, 1755 ZG Petten, The Netherlands
[5]CRES Wind Energy Department, 19th Km Marathonos Avenue, 190-09, Pikermi, Greece

ABSTRACT

There seems to be a significant uncertainty in aerodynamic and aeroelastic simulations on megawatt turbines operating in inflow with considerable shear, in particular with the engineering blade element momentum (BEM) model, commonly implemented in the aeroelastic design codes used by industry. Computations with advanced vortex and computational fluid dynamics models are used to provide improved insight into the complex flow phenomena and rotor aerodynamics caused by the sheared inflow. One consistent result from the advanced models is the variation of induced velocity as a function of azimuth when shear is present in the inflow. This gives guidance to how the BEM modeling of shear should be implemented. Another result from the advanced vortex model computations is a clear indication of influence of the ground, and the general tendency is a speed up effect of the flow through the rotor giving a higher power than in uniform flow. On the basis of the consistent azimuthal induction variations seen in the advanced model results, three different BEM implementation methods are discussed and tested in the same aeroelastic code. A full local BEM implementation on an elemental stream tube in both azimuth and radial direction seems to be closest to the advanced model results. Copyright © 2011 John Wiley & Sons, Ltd.

KEYWORDS

BEM; sheared inflow; induction; rotor aerodynamics; ground effect

Correspondence

H. Aa. Madsen, Wind Energy Division, Risø DTU, Building 118, DK-4000 Roskilde, Denmark.
E-mail: hama@risoe.dtu.dk

Received 19 August 2010; Revised 15 April 2011; Accepted 2 May 2011

NOMENCLATURE

a	induction coefficient
B	number of blades
C_p	rotor power coefficient
C_T	local thrust coefficient
C_y	projection of lift and drag coefficient in streamwise direction
FN	normal force per blade length on airfoil section (N m^{-1})
FT	tangential force per blade length on airfoil section (N m^{-1})
r	radial position
u_{in}	axial induced velocity
V_∞	free stream velocity (m s^{-1})
V_{ref}	normalization velocity for local thrust coefficient (m s^{-1})
$V_{ref\text{-}av}$	mean free stream velocity with an annular stream tube
W	flow relative velocity relative to blade section (m s^{-1})
θ	azimuth position

Copyright © 2011 John Wiley & Sons, Ltd.

1. INTRODUCTION

With the increasing size of wind turbines with rotor diameters for the largest turbines above 120 m, the variation of the mean wind speed over the rotor height due to wind shear can be considerable. Likewise, wind shear can be caused by the wakes from upstream turbines, and in this case, the main variation of the inflow velocity will often be in a horizontal direction. An additional characteristic with shear due to wakes is that it is a quite dynamic inflow situation due to meandering of the wakes, which means that the velocity deficit moves around in a plane perpendicular to the main flow direction. Finally, shear is also due to the large scales in the atmospheric turbulence, and in high turbulence conditions, the instantaneous wind speed can be quite different from one side of the rotor to the other.

It seems that there is a significant uncertainty in computing rotor power and loads under such conditions, in particular with the engineering codes based on the blade element momentum (BEM) theory, commonly implemented in the aeroelastic design codes used by industry. The BEM model for induction computations is originally based on a stream tube continuity and momentum balance for uniform flow through the rotor. An important extension was presented by Glauert,[1] assuming that the equation relating the thrust coefficient to the induction can be used on an elemental (radial direction) annular stream tube. Glauert mentions that the equation has not been proven and the uncertainty is related to a possible interaction between the stream tubes. The conclusion by Glauert is, however, that the uncertainty in general by using the differential form of the equation is small. The differential version of the BEM model was the basis for a number of later formulations of what also has been denoted as 'the strip theory', e.g., derived by Wilson[2] and de Vries.[3] These classical references of the engineering BEM model implementations do also contain a discussion of inflow with wind shear. Using as a starting point the steady state BEM-based equations for the different rotor forces and moments, e.g., rotor torque and tilt moment, Wilson[2] derived linearized expressions for the variations of these forces and moments due to wind shear by use of a Taylor expansion from the conditions at hub height. Applying finally a number of approximations such as constant chord and lift coefficient on the outer part of the blade, Wilson found a closed form solution for the torque variations due to wind shear. As an example, Wilson inserted turbine specific data for the 175 ft diameter Smith-Putnam turbine and computed a decrease in mean power output of about 3% for a wind shear following the power law of 1/6.

De Vries[3] derived somewhat similar equations for the influence of wind shear but using as a starting point the theory of Glauert[4] for the effect of sideslip and pitching of a propeller. However, de Vries concluded that the analytical expressions are so complicated and still derived under a number of assumptions that a numerical approach using the BEM method is preferable. In fact, de Vries then briefly described a computational approach for sheared inflow by computing with the BEM method the induction for different azimuth blade positions and at each position assumed axisymmetric wind conditions. Finally, the rotor power and loads were derived by combining properly the results for different rotor positions. De Vries added: 'a lot of aspects have been ignored in this approach (e.g. unsteady effects)'.

It is thus uncertain how accurate the BEM model can compute the induction for complex inflow cases, and there is also a lack of detailed model description of how to implement the BEM model for non-uniform and turbulent inflow conditions. Although all the major aeroelastic codes used by industry, e.g., FLEX5(4),[5] BLADED,[6] HAWC2,[7,8] FAST[9] and General Aerodynamic and Structural Prediction Tool (GAST),[10] used the BEM model, different implementations seem to be used, and the model results will differ.

As concerns modeling of sheared inflow with advanced flow models such as full 3D computational fluid dynamics rotor models, published studies and results have until recently been sparse. This is, e.g., due to the huge requirements to the grids, which in the case of an atmospheric boundary layer shall resolve this as well as the boundary layer on the blades representing big differences in scale. When the atmospheric boundary layer is resolved, it is then often in combination with a less detailed model of the rotor such as an actuator disk.

The subject of improving the aerodynamic and aeroelastic modeling of megawatt (MW) rotors using realistic non-uniform and unsteady inflow has been one of the five research themes in Work Package 2 (WP2) of the European UpWind Project, and the results presented in the present paper are based on this work. The uncertainty in computing the aerodynamic forces for these common inflow cases is a limitation for the further optimization and design of MW turbines. One area of influence is the impact on development of new individual blade pitch control algorithms to alleviate fatigue loads, e.g., in wind farm operation that requires accurate computation of the aerodynamic loads. Another area of uncertainty from sheared inflow is the power curve measurements where it is unclear if periods with strong shear in inflow should be let out because of possible changed power coefficient for the turbine. Although the research work in WP2 comprises all the three different types of sheared flow mentioned above, it is mainly the sheared atmospheric inflow that is considered in the present study.

The content of the paper is structured in a way that, first, some examples of measured shear in inflow to MW turbines are shown and discussed in Section 2. Then, in Section 3, a presentation of the models used in the study and of the test case. Results are presented and commented in Section 4, followed by a deeper discussion of the different flow phenomena and rotor aerodynamics resulting from sheared inflow in Section 5. Three different BEM implementation methods are presented in Section 6 together with numerical test results from using the different methods in the same aeroelastic code. Finally, the ground effect is investigated in Section 7.

Wind Energ. 2012; **15**:63–81 © 2011 John Wiley & Sons, Ltd.
DOI: 10.1002/we

2. EXPERIMENTAL EVIDENCE OF SHEARED INFLOW

2.1. Atmospheric sheared flow

The measured wind speed at six different heights at the wind turbine Test Site at Høvsøre in Denmark during a period of 1 day is shown in Figure 1.[11] During the night, the atmospheric boundary layer is quite stable, and a considerable shear is developing with a difference in wind speed of about 5 m s^{-1} from a height of 40 to 116 m. Also, a considerable variation in wind direction as a function of height is seen in the lower part of Figure 1.

During the same period, the local inflow angle at a blade radial position of 36 m on the Siemens 3.6 MW turbine (Siemens Wind Power, Borupvej 16, 7330 Brande, Denmark) was measured.[11] The variation of the local inflow angle (mean value not calibrated) as a function of blade azimuth position is shown in Figure 2 at four different times, binned over a period of 10 min, during the morning hours.

At 08:00 h, there is a considerable variation of about 7° during one revolution, but during the next 4 h, this variation reduces considerably, and correlating with the meteorology mast data in Figure 1, it is the same period where the wind shear almost disappears.

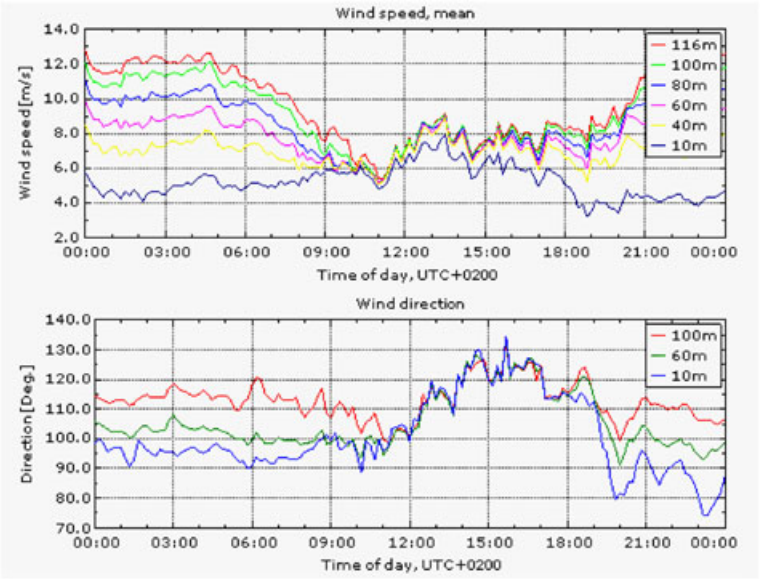


Figure 1. Wind speed and wind direction measured over 1 day (March 27, 2007) at the Høvsøre wind turbine test site in Denmark. Data are from Madsen and Fischer.[11]

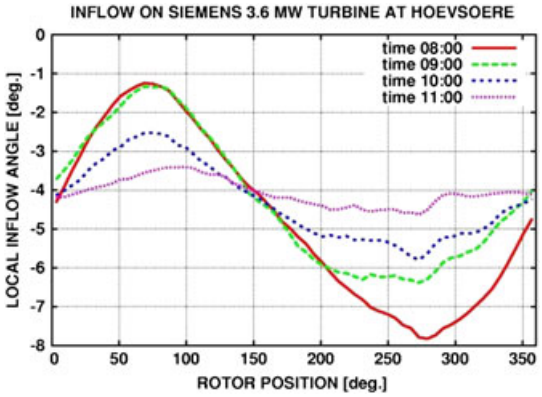


Figure 2. Measured local inflow angle with a five hole pitot tube at 36 m radius on the Siemens 3.6 MW turbine on the test site measured at different times during the same day as the wind data in Figure 1. Data are from Madsen and Fischer.[11]

The wind data have been monitored over a longer time at the Høvsøre test site and Antoniou *et al.*[12] presented the results of analysing and categorizing the different wind shear profiles over a period of 1 year as shown in Figure 3. For the most frequent wind shear profiles there is a difference in wind speed of 3 m s^{-1} from height 40 m to height 160 m which is comparable to the diameter of a MW turbine like the Siemens 3.6 MW turbine on the site. It is also seen that for the most extreme wind shear category the difference in wind speed from bottom to top is close to 5 m s^{-1}.

2.2. Wind shear due to wakes

Another major cause of shear in inflow is wake operation. An example of this was presented by Madsen *et al.*[13] and is shown in Figure 4. The measured variation in local inflow angle at about 60% radius on a 2 MW turbine operating in half wake and about 3.5D downstream the wake generating turbine is shown. Again, a considerable variation of the local inflow angle is seen, causing a substantial variation of the flapwise blade root moment.

3. APPROACH

An evaluation of the uncertainty of the engineering BEM type aerodynamic and aeroelastic codes was carried out by comparing their results with the results of more advanced codes, although these do not necessarily represent the correct results. A comprehensive comparison was carried out within the WP2 of the UpWind Project and reported in a task report.[14] The turbine used as test case is the 5 MW reference (REF) turbine defined by Jonkman *et al.*[15]

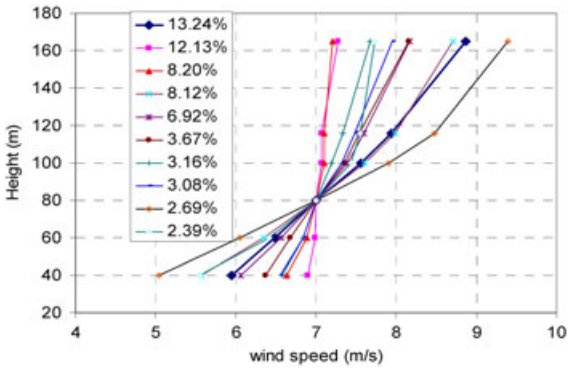


Figure 3. The 10 most common normalized wind shear profiles and their percentage of occurrence measured over 1 year at the Høvsøre test site. Figure is from Antoniou *et al.*[12]

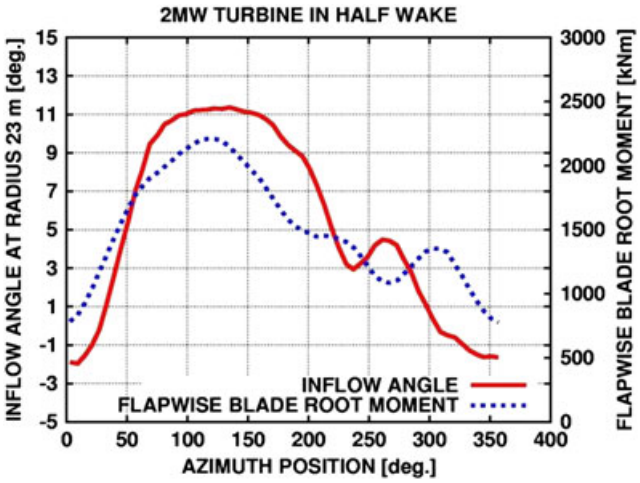


Figure 4. Measured local inflow angle in a radius of 24 m on a 2 MW turbine and compared with the flapwise blade root bending moment during half wake operation. Figure is from Madsen *et al.*[13]

Wind Energ. 2012; **15**:63–81 © 2011 John Wiley & Sons, Ltd.
DOI: 10.1002/we

3.1. The codes

Below, the codes are grouped according to their details in modeling the flow:

Computational fluid dynamics codes

- The EllipSys3D code [Risø Danish Technical University (DTU) and DTU Mekanik (DTU MEK)][16–18]
- The Actuator Line (ACL) code (DTU MEK)[19] using the EllipSys3D as flow solver

Vortex codes

- The GENeralized Unsteady Vortex Particle (GENUVP) code [National Technical University of Athens (NTUA), Centre for Renewable Energy Sources (CRES)][20]
- The Aerodynamic Windturbine Simulation Module (AWSM) code [Energy Research Centre of the Netherlands (ECN)][21–23]

BEM codes

- The FLEX5 code (DTU MEK)[5]
- The GAST code (NTUA, CRES)[10]
- The HAWC2 code (Risø DTU)[8]

Details on EllipSys3D modeling

The EllipSys3D is an incompressible Navier–Stokes flow solver formulated as a finite volume discretization of the Reynolds-averaged Navier–Stokes (RANS) equations. The present simulations were all carried out as unsteady simulations using the Pressure Implicit solution by Split Operator method (PISO) algorithm to solve the coupled momentum and pressure-correction equations. The convective terms were discretized using the Quadratic Upwind Interpolation for Convective Kinetics (QUICK). The flow over the blades was assumed fully turbulent and modeled using the $k-\omega$ Shear Stress Transport turbulence model by Menter. The relative motion between the rotor and the ground was handled using the overset grid method, which allows for the decomposition of a domain into smaller grids that are allowed to overlap and move relative to each other. Communication of flow field quantities between the individual grids was carried out using trilinear interpolation.

Two computational domains were made: one with a ground boundary corresponding to a hub height of 90 m and another domain with the ground boundary placed five rotor diameters away from the rotor center. The domain with the ground boundary placed far away from the rotor was used solely for the uniform inflow case. The rotor was fully resolved using 256 cells in the chordwise direction and 128 cells in the spanwise direction. The height of the first cell in the boundary layer was 1×10^{-6} corresponding to a $y+$ of less than 2. The mesh resolving the remainder of the domain was refined in the wake region to resolve the tip and root vortices sufficiently. The total number of cells was 15×10^{6}. The outer boundaries of the computational domain extended 8 rotor diameters upstream, 10 diameters downstream, and 8 diameters in the radial direction. For more details on the computational method, see Zahle.[24]

It should be noted that EllipSys3D is the only code in the present study where just the blade geometry and the operational conditions are the input data. The other codes need airfoil data, but in the present case, exactly the same data set have been used for all the codes.

Details on the ACL modeling

In the ACL computations, a computational grid of 5.97 million cells was used. The grid is made so that at the position of the rotor, the grid consists of cubes, and the local grid density allowed that a blade could be divided into 31 spanwise sections. The time increment is made so that for each time step the actuator line moves no more than one cell. In the ACL model, the boundary layer on the solid walls on the blades is not resolved so that only large eddies are created at the rotor, and a large eddy simulation model was used to model turbulent eddies becoming smaller than the grid. As the detailed flow around the blades was not resolved, the blade forces were derived on the basis of a local inflow angle and a relative velocity at each blade section in combination with airfoil data as in the BEM codes.

3.2. The shear and ground modeling

The GENUVP and the AWSM models have been used specifically to study the influence of the ground in combination with different tower heights. Results on this will be presented in Section 7.

ACL model

Simulations were only run for cases with the ground present, and the shear was generated by the use of body forces as described by Mikkelsen *et al.*[25]

The EllipSys3D model

The model was run with and without the ground present. The ground boundary was enforced using a slip (symmetry) wall.

Using RANS, it is not possible to prescribe a turbulent inflow since the turbulent eddy viscosity in an atmospheric boundary layer is several orders of magnitude larger than that developing in the boundary layer on the blade surfaces. Thus, a simulation combining a turbulent shear with a rotor simulation would result in the rotor operating in an extremely low effective Reynolds number. As such, the sheared velocity profile prescribed at the inflow boundary was assumed to be essentially laminar.

Simulations with a sheared inflow required a very long simulation time to converge, perhaps because of the low flow velocity in the lower part of the shear combined with the unsteady nature of the wake. This necessitated the use of the grid sequencing and time step sequencing capability of EllipSys3D, by first computing the flow on the mesh coarsened by a factor of 2 in each coordinate direction with a very coarse time step with 150 time steps per revolution for 20 revolutions. The time step was subsequently refined by a factor of 10 yielding 1500 time steps per revolution that ran for 15 revolutions. Finally, the mesh was refined to the finest mesh, and the time step was refined by a factor of 2 to $\Delta t = 2.173 \times 10^{-3}$. As shown in Figure 5, the rotor torque convergence of the shear flow simulation was quite slow and continued to exhibit unsteady behavior also at the finest grid level. However, as is evident, the solution on grid level 2 compared well with the fine grid solution.

GENUVP model

The shear profile was applied to the inflow (free stream velocity) upstream of the turbine where the disturbances from the rotor and the wake vanished. The shear profile was continued down to height 0. In the case where the ground effect is not taken into account, if any vortex particle passes outside this boundary surface, they are set to be transported with an axial velocity of 0.1 m s^{-1}.

In the GENUVP model, the effect of the ground was introduced by satisfying non-entry boundary condition on the ground level. This was done by applying the mirroring technique as illustrated in Figure 6. A contra-rotating rotor was introduced below the ground level at a distance equal to the hub height of the rotor. Because of the opposite sign of its rotation with respect to the original rotor, the circulation over the blades and the vorticity of the wakes will also be oppositely directed. This implies that non-entry condition is by definition satisfied on the symmetry plain. Also, the shear profile was extended below the ground level, as shown in Figure 6.

The AWSM model

In the AWSM model, which is based on Prandtl's lifting line theory, the ground was 'virtually' taken into account by mirroring each influencing point on the lifting lines. More specifically, the location of each mirrored point was opposite to the original one compared with the location of the ground, and the circulation was also inverted in sign.

3.3. The inflow test case

A test case at 8 m s^{-1} was chosen because it is typically the wind speed where the turbine operates at maximum power coefficient C_p and because it is around the most frequent wind speed for the complete operational interval. Further, it has

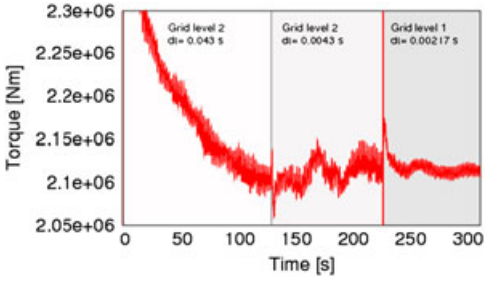


Figure 5. Convergence of the rotor torque for the fully resolved rotor simulation with sheared inflow.

Wind Energ. 2012; **15**:63–81 © 2011 John Wiley & Sons, Ltd.
DOI: 10.1002/we

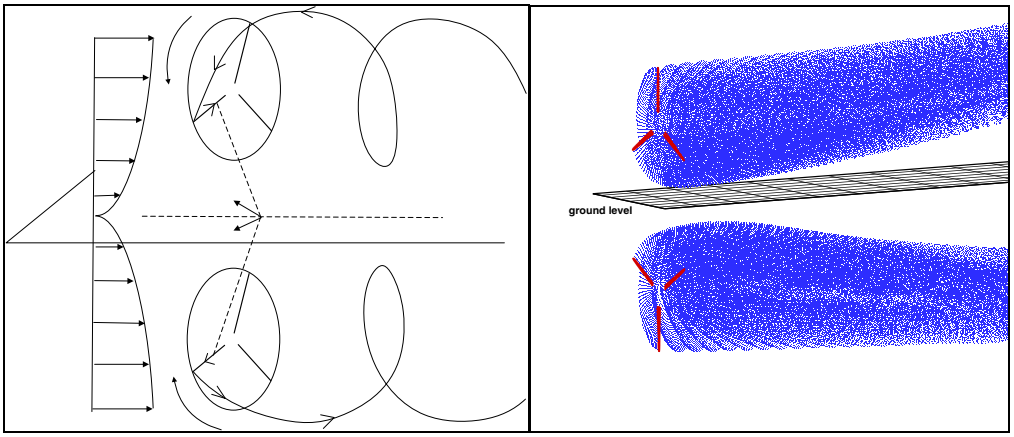


Figure 6. The ground modeled in the GENUVP model using a mirror technique.

been an objective to avoid any major influence from stall on the blades. An extreme wind shear following the power law with an exponent of 0.55 has further been selected for the investigation as shown in Figure 7 for a tower height of 90 m. The following data for mean values over the rotor disk can be derived:

- Mean wind speed of 7.85 m s^{-1}, which is 2% lower than the hub wind speed and the uniform flow wind speed of 8 m s^{-1}.
- Mean V^2 is the same as for the uniform flow field.
- Mean V^3 is 5.8% higher than for the uniform flow field.

4. RESULTS

4.1. Uniform inflow

The codes were first compared for the uniform inflow case in order to evaluate the differences for the most simple inflow conditions. The distribution of normal and tangential force and normal and tangential induction is compared in Figure 8. In general, there is a very good correlation for both the tangential and normal forces, and the deviation of the ACL model results is due to a different implementation of the tip correction model.[26] In principal, no tip correction model is needed in the ACL computations since the loads are distributed along the lines defined by the actual position of the blades. However, if the grid density is too coarse to resolve the full tip vortex, something is missing with respect to the induction close to the tip. As the grid is refined, the ACL solution near the tip is approaching more the BEM results including Prandtl's tip loss

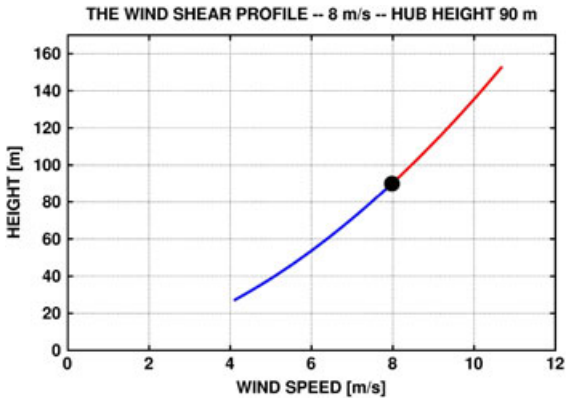


Figure 7. The wind shear used for the numerical simulations.

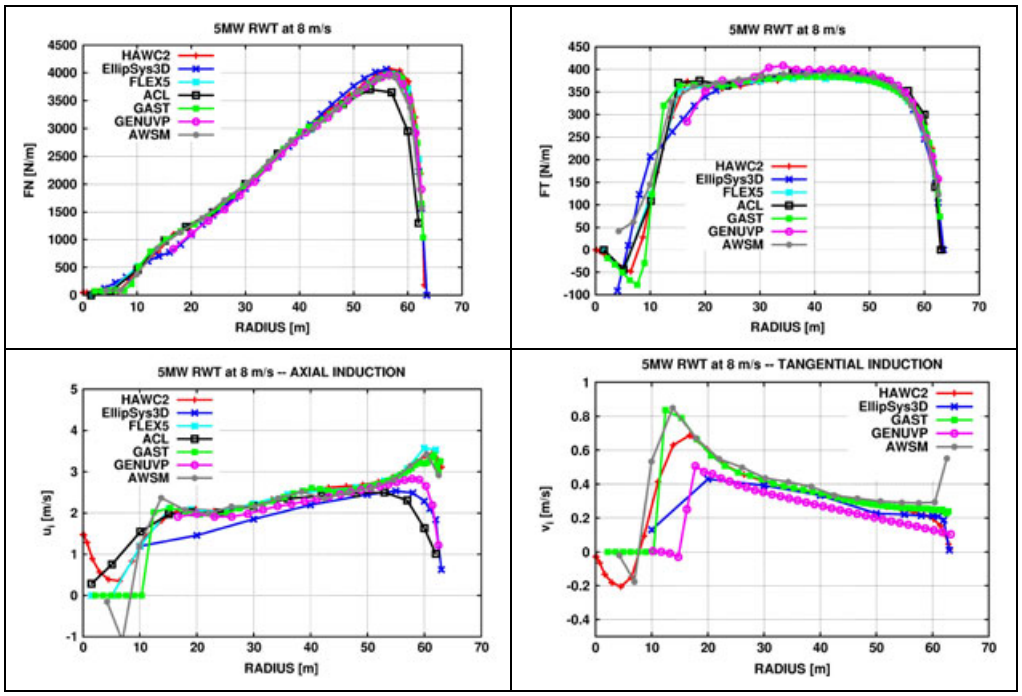


Figure 8. Blade load distribution and induction computed with the different models for uniform inflow.

correction. It would therefore be tempting to try and model what is missing with respect to the tip vortex, but such model is not trivial since it should be a function of the grid density.

There are also small deviations for the tangential forces in the range from 10 to 20 m where the EllipSys3D results are lower than the majority of the other results, but this can probably be ascribed to partial stall modeled more accurately by the EllipSys3D code compared with the models relying on input airfoil data.

As concerns the induced velocities shown in the lower part of Figure 8, the correlation between the models is also quite good except in the tip region. However, these deviations are due to the tip correction applied in the BEM type models giving a local induction, whereas for the EllipSys3D code, it is the mean induction over time that is shown.

4.2. Inflow with shear

Next, computations for inflow with shear were compared. It should be noted that all the advanced codes were run with the ground present although this is not modeled in the BEM type codes. The case with ground was chosen because it was not possible to simulate the shear without the ground in the case with the EllipSys3D code as the lower boundary had to be specified much further away than at height 0 m, where the velocity profile is defined down to.

The computed load distributions for two blade azimuth positions (position 0° is vertical upwards) for inflow with shear are shown in Figure 9. Considerable deviations between the models' results of up to 20–30% are now seen for the load distributions and in particular for the tangential force. In general, the correlation between the results from the advanced models is better than for the three BEM based codes. However, like for the uniform inflow case, the tip correction modeling causes deviations for the ACL results and in particular for the normal forces distribution for the blade position of 0°. The tendency for the BEM type based codes is that the GAST and HAWC2 results are close to each other but deviate considerably to the FLEX5 results, indicating a different implementation of the BEM model to handle inflow with shear.

The corresponding axial induction results are shown in Figure 10, and as for the loads, the correlation between the advanced model results is better than for the BEM models. The deviations for the BEM type models are biggest for blade positions 0° and 180°.

Finally, the integrated values of rotor power and thrust for the different computations are compared in Table I. The results from the BEM based code Blade Optimization Tool (BOT)[27] from ECN has also been included in this table. For the no shear case, the maximum deviation in computed power is around 1% and somewhat the same for the thrust except for the GENUVP model, in which the root of the blade (non-aerodynamic part) is not modeled and, therefore, thrust is expected to

Wind Energ. 2012; **15**:63–81 © 2011 John Wiley & Sons, Ltd.
DOI: 10.1002/we

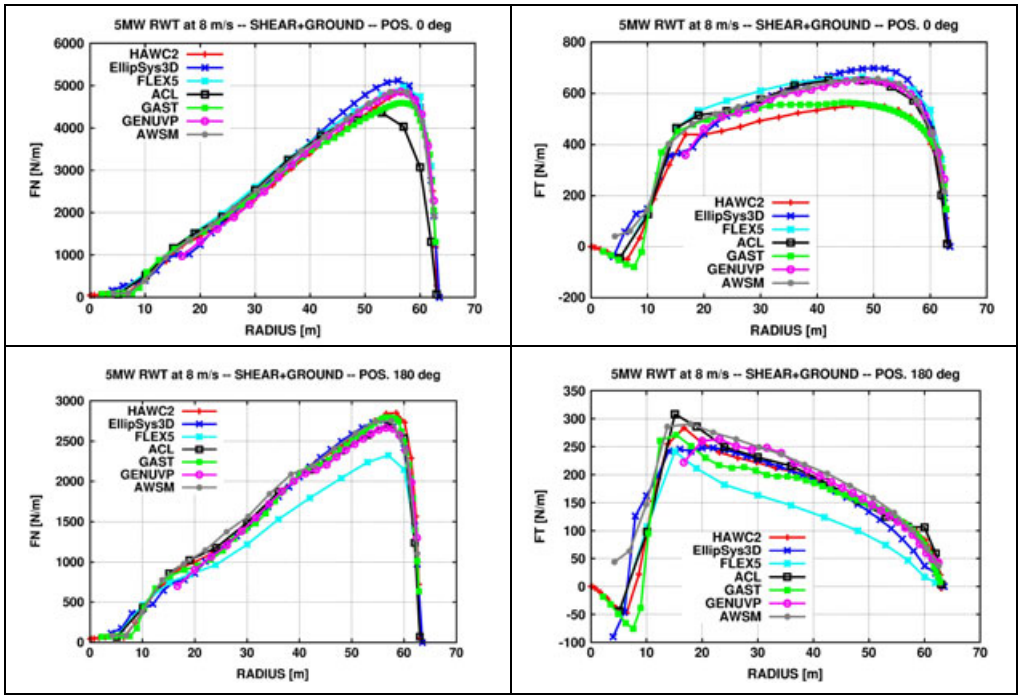


Figure 9. Blade load distribution for two blade positions (blade vertical up and vertical down, respectively) computed with the different models.

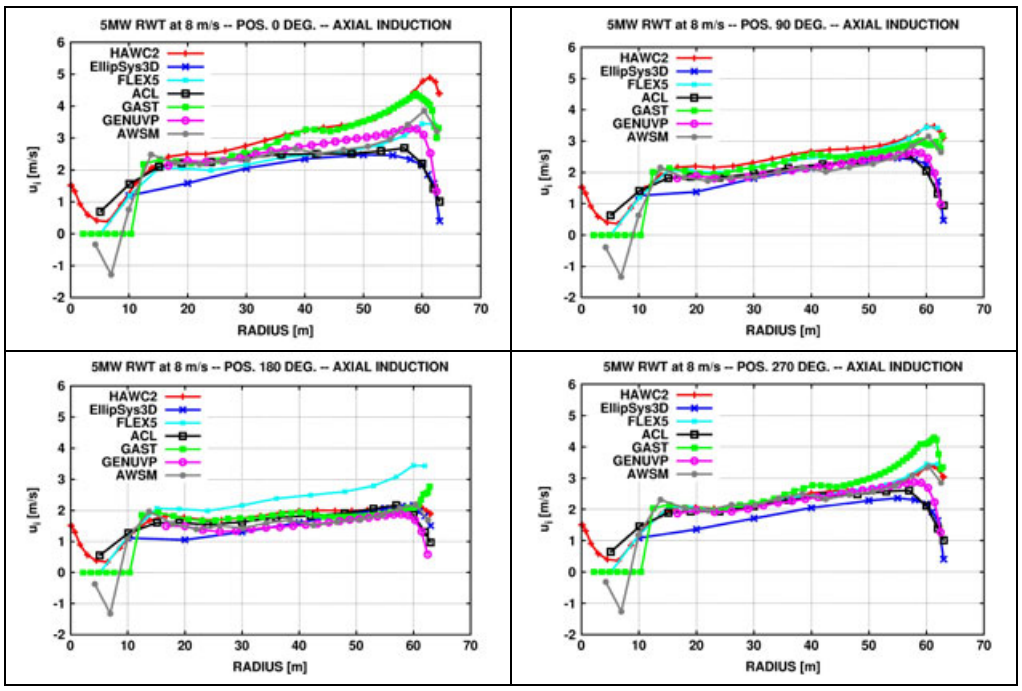


Figure 10. Axial induction for four blade positions computed with the different models.

Table I. Integrated values of rotor power and rotor thrust for the different cases.

	HAWC2	EllipSys3D	FLEX5	ACL	GAST	GENUVP	AWSM	BOT
Power (kW), no shear	1928	1937	1958	1958	1934	1917	1953	1931
Power (kW), shear+ (ground)	1855	2036	1958	1942	1855	1971	2078	
% rel. to no shear	−3.8	5.1	0.0	−0.8	−4.1	2.8	6.4	
Thrust (kN), no shear	391	387	386	374	387	362	382	386
Thrust (kN), shear+ (ground)	380	388	376	370	374	360	386	

be somewhat lower. However, for the shear case, the spreading in the results is bigger, ranging from an increase in power for the sheared inflow of 6.4% (AWSM) to a small decrease in power of 0.8% (ACL). The two BEM based codes HAWC2 and GAST show a considerable decrease in power, whereas FLEX5 computes the same power for the uniform inflow. The possible causes for these deviations and the flow mechanisms behind will be discussed in the next section.

5. DISCUSSION OF SHEARED FLOW MECHANISMS AND ROTOR AERODYNAMICS

A number of different flow mechanisms as concerns the rotor aerodynamics and the energy conversion are caused by the sheared inflow. The induction varies over the rotor disk; the operational point for the individual airfoil sections varies during one rotor revolution; the wake rotation behind the rotor causes a redistribution of the sheared flow, and the vortex sheets behind the rotor are tilted. These effects will be exemplified and discussed below in order to come closer to an understanding of how the sheared flow influences the energy conversion and the loading on the rotor. This will also lead to a better understanding of the difference in the comparison of results in Section 4. The influence of the ground will be considered in more detail in the Section 7.

5.1. Varying induction characteristics over the rotor

To get a first insight into the variation of the induction over the rotor disk, we run a HAWC2 BEM simulation with uniform inflow at three different wind speeds (10.8, 8 and 4.1 m s^{-1}) corresponding to the wind speed at top, mid and bottom positions of the blade tip but for the same rotor speed in all three cases corresponding to the nominal value at 8 m s^{-1}. It is seen in Figure 11 that the thrust coefficient on the outer part of the blade varies a lot from a typical value of 0.7 for the 10.8 m s^{-1} case to about 1.5 for the low wind speed case. This shows that the turbine is in a quite different operational condition from the top part of the rotor disk to the bottom part. However, when comparing the induced axial velocities shown in the right part of Figure 11, it is seen that the differences are much less, which is because of the strong non-linear correlation between thrust coefficient and induced velocity at high loading.

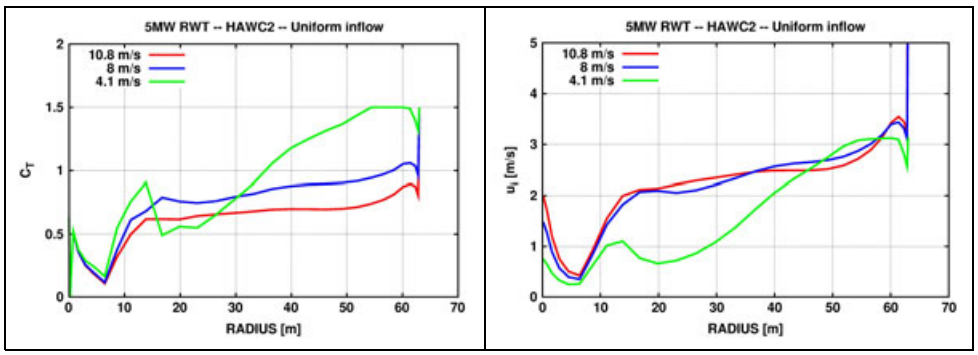


Figure 11. BEM simulation on a rotor with uniform inflow at three different wind speeds corresponding to the wind speed at the top of the rotor in sheared flow (10.8 m s^{-1}), at hub height (8 m s^{-1}) and at the bottom of the rotor (4.1 m s^{-1}), respectively, and with the same rotational speed in all three cases.

Wind Energ. 2012; **15**:63–81 © 2011 John Wiley & Sons, Ltd.
DOI: 10.1002/we

5.2. Induction characteristics from advanced model results

For each of the advanced models, the axial induction for the blade in the four positions is extracted from Figure 10 and shown in Figure 12 to illustrate the induction dependency on azimuth for each model. Although the computed induction by the different models differs somewhat in mean level, some clear tendencies can be found:

- The induction is bigger for the blade in the top position compared with the down position.
- For most of the models, this difference is rather constant along the blade and is around 1 m s^{-1}.
- When comparing the data for positions 90° and 270°, there is a small difference indicating that there is a hysteresis effect in the induction. However, for the EllipSys3D results, the induced velocity is slightly higher in the 90° position compared with the 270° position, but for the other three models, the tendency is opposite.

The advanced model results indicate, thus, that the BEM should be implemented in a way to allow a variation of the local induction as a function of azimuth position at a constant radial position.

5.3. Variation of operational point for the airfoil sections

The result of the variation of the inflow velocity over the rotor disk will be different operational points for the airfoil sections along the blade. In order to investigate this effect on the rotor power, we run a simulation with the HAWC2 code, and in order not to have the results influenced by the uncertainty of induction, we run both simulations without computation of induction but at a reduced free wind speed of 5.28 m s^{-1} (0.66×8 m s^{-1}) corresponding to a constant induction factor of 0.33 over the rotor.

The lift/drag ratio at two radial positions is shown in Figure 13. For the case with sheared inflow, a considerable variation of angle of attack is seen and, likewise, a variation in lift/drag ratio. For the radial position of 37 m, the blade is close to operation at the maximum value in uniform inflow. The sheared inflow will therefore lead to a lower mean value of lift/drag ratio. For the 54 m radial position, the 8 m s^{-1} uniform operational point is somewhat more away from the optimal position, but still the inflow variations in sheared flow will again lead to a lower mean lift/drag ratio.

It is thus expected that the general influence of the varying operational point for the airfoil sections will lead to a decrease in rotor power, and this is also what is seen in the present case. For the uniform inflow, the computed power was 1868 and 1835 kW for the sheared inflow case, and this should be seen in relation to the 5.8% higher power in the inflow with shear.

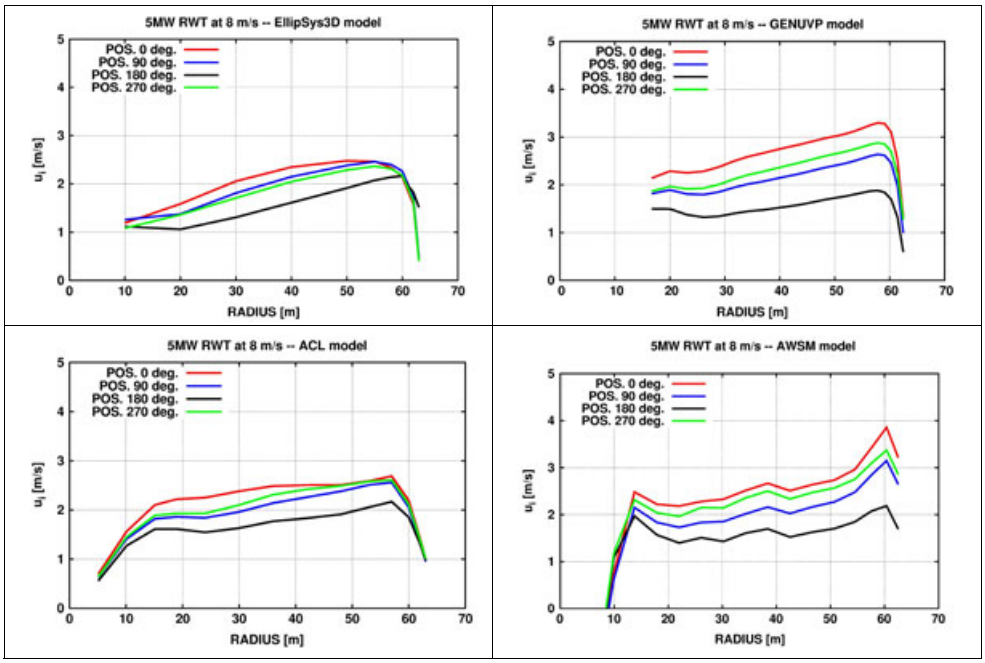


Figure 12. Axial induction for the four blade position computed with the four advanced models.

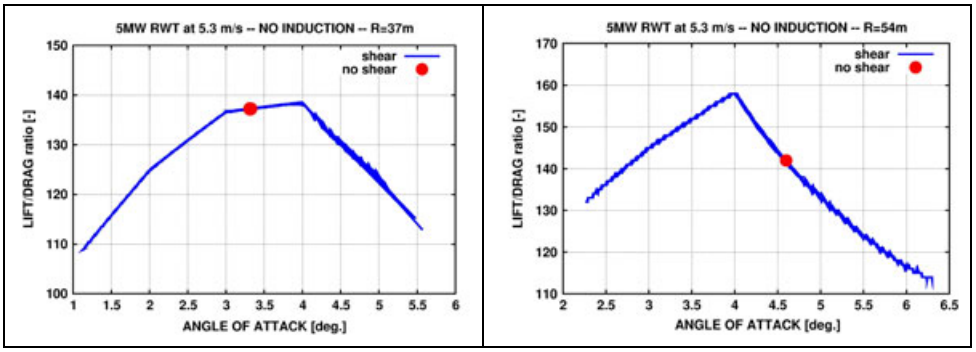


Figure 13. Variation of lift/drag for an airfoil section at a radius of 45 m for sheared flow and for uniform flow, respectively, at a hub height wind speed of 5.28 m s^{-1} and without induction.

5.4. Wake rotation

The swirl in the wake is expected to have a considerable influence on the axial flow velocity contours as a function of downstream position in the wake when shear is present in the inflow. This is illustrated on the basis of the EllipSys3D results with the two contour plots shown in Figure 14 that shows that the axial velocity contours at the rotor disk slowly turn in the opposite direction of the rotor rotation, and for the downstream distance of 3D, the rotation is almost 90° as seen in the right plot of Figure 14. It could have influence on the induction in the rotor plane and, e.g., lead to differences in the induction for the blade in position 90° and 270°, which is not accounted for in BEM models. The asymmetry in the wake from a turbine operating in shear will also influence the wake-induced loads on downstream turbines depending on the relative distance.

5.5. Other flow effects

The variation of the axial velocity in the wake as a function of height means that the vortex sheets from the rotor are tilted as the transport velocity in the top is bigger than in the bottom of the wake. This is clearly seen in the computations by the GENUVP model, illustrated by the position of the individual vortex elements for sheared inflow shown in Figure 15. The vortex sheets are tilted considerably short after the rotor disk, and this is probably the cause of the upward movement of the wake due to the induced upward velocity component of the tilted vortex sheets. Another flow effect by the sheared inflow is presented and discussed by Troldborg *et al.*[28] on the basis of a simplified analytical vortex model and a full Navier–Stokes simulation using the actuator disk to model the rotor. The flow effect is a downward induced velocity caused by the vorticity of the sheared flow, which is transported slower when passing the rotor and entering the wake compared with the flow outside the wake. The deformation of the vortex field by the wake will cause a downward induced velocity in front of the rotor disk and at the rotor disk with the result that the flow entering the rotor disk is originating from a slightly higher vertical position and thus has a higher axial velocity due to the shear. The effect is a higher power coefficient of the

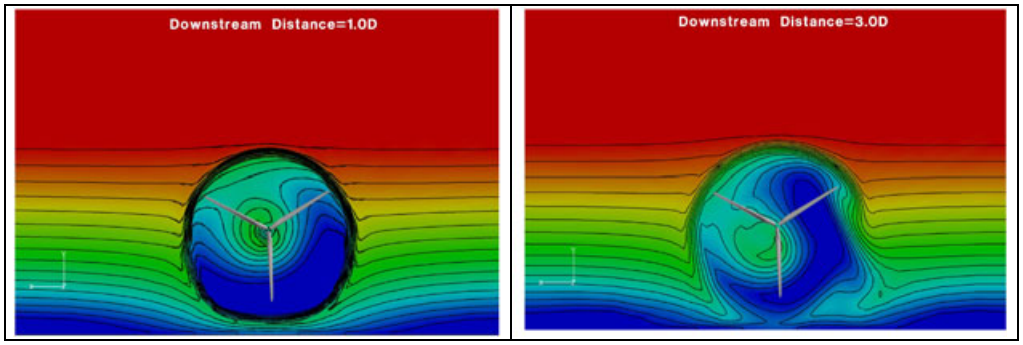


Figure 14. Axial velocity contour plot at two down downstream positions from EllipSys3D computations.

Wind Energ. 2012; **15**:63–81 © 2011 John Wiley & Sons, Ltd.
DOI: 10.1002/we

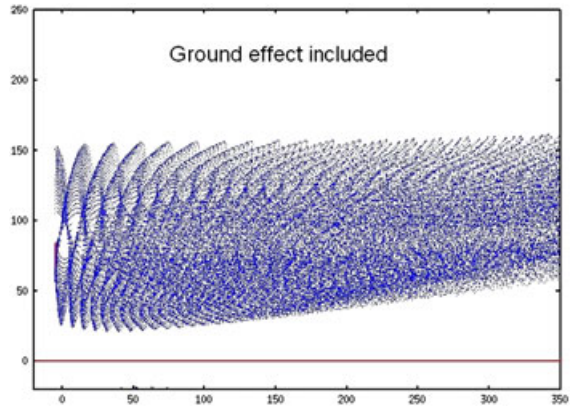


Figure 15. The vortex sheets, illustrated by the position of the vortex elements released at each time step, computed with the GENUVP model for sheared inflow.

rotor and in particular on the lower part of the rotor disk. The results from the analytical model are confirmed by actuator disk simulations with a prescribed loading on the disk. The tendency of the flow to be diverted downwards in a shear is also observed in the present simulations using EllipSys3D with a fully resolved rotor geometry, which is discussed in more detail in Zahle.[24]

5.6. Discussion

The above-mentioned different flow effects from the sheared inflow have been discussed. Some of them tend to decrease the rotor power coefficient (non-optimal loading/induction and the operational point for the airfoil sections), whereas the effect described by Troldborg *et al.*[28] increases the rotor power coefficient. The influence from other effects is uncertain, e.g., the rotation of the wake. This illustrates the complex case of computation of power and loading for a rotor in sheared flow and should be in mind when evaluating the different results on power and thrust for the rotor in sheared inflow as presented above. However, it should also be recalled that the power content of the sheared inflow is about 6% higher than for uniform flow, which means that the different mechanisms decreasing the power shall have substantial effect in order to counteract the increased power content. Finally, the ground effect, another important parameter, is still to be discussed in Section 7.

6. BEM IMPLEMENTATIONS FOR INFLOW WITH SHEAR

We have seen above that the different implementations of the BEM model give almost identical results for uniform inflow, but for the shear flow case, bigger deviations are seen. Without going into a detailed discussion of the BEM implementation in the different codes, a brief, general illustration of the problem is presented.

6.1. Different implementations of the BEM model

We can define a local thrust coefficient $C_{\mathrm{T}}(\theta, r)$ as

$$C_{\mathrm{T}}(\theta, r) = \frac{\frac{1}{2}\rho W^2(\theta, r)\, C_y(\theta, r)\; c\; B\, \mathrm{d}r}{\frac{1}{2}\,\rho\, V_{\mathrm{ref}}^2(\theta, r)\; 2\,\pi\, r\, \mathrm{d}r} \tag{1}$$

where W is the relative velocity to the blade section, ρ is the density of mass, C_y is the projection of the airfoil lift and drag coefficient in the axial direction, θ is the azimuth position, B is the number of blades and V_{ref} is a reference wind speed.

Equation (1) can be reduced to

$$C_{\mathrm{T}}(\theta, r) = \frac{W^2(\theta, r)\; C_y(\theta, r)\; c\; B\, \mathrm{d}r}{V_{\mathrm{ref}}^2(\theta, r)\; 2\,\pi\, r\, \mathrm{d}r} \tag{2}$$

For the uniform inflow case, the variables will not be a function of azimuth, the reference wind speed will be equal to the free wind speed V_∞ and equation (2) reduces to

$$C_{\mathrm{T}}(r) = \frac{W^2(r)\ C_y(r)\ c\ B\,\mathrm{d}r}{V_\infty^2\ 2\,\pi\,r\,\mathrm{d}r} \tag{3}$$

Then, we can derive the induction $a(r)$ from

$$C_{\mathrm{T}}(r) = 4\,a(r)\ [1 - a(r)] \tag{4}$$

and finally compute the induced velocity $u_{\mathrm{in}}(r)$ by

$$u_{\mathrm{in}}(r) = V_\infty\, a(r) \tag{5}$$

However, for the inflow with shear, we are back with equation (2), and some choices must be taken. Three different implementations, BEM1, BEM2 and BEM3, are presented here.

BEM1

$$C_{\mathrm{T}}(r) = \frac{\sum_{i=1}^{B} W^2(\theta_i, r)\ C_y(\theta_i, r)\ c}{V_{\text{ref-av}}^2(r)\ 2\,\pi\,r} \tag{6}$$

where θ_i is the azimuth position of blade no. i and $V_{\text{ref-av}}$ is the mean free stream velocity within the stream tube at the radial position r.

BEM2

$$C_{\mathrm{T}}(\theta, r) = \frac{W^2(\theta, r)\ C_y(\theta, r)\ c\ B\,\mathrm{d}r}{V_{\text{av-disk}}^2\ 2\,\pi\,r\,\mathrm{d}r} \tag{7}$$

where $V_{\text{av-disk}}$ is the mean value of the inflow velocity to the rotor disk.

The induced velocity is then derived as

$$u_{\mathrm{in}}(r, \theta) = V_{\text{av-disk}}\, a(r, \theta) \tag{8}$$

and $a(\theta, r)$ is derived from the equation

$$C_{\mathrm{T}}(\theta, r) = 4\,a(\theta, r)\ [1 - a(\theta, r)] \tag{9}$$

BEM3

$$C_{\mathrm{T}}(\theta, r) = \frac{W^2(\theta, r)\ C_y(\theta, r)\ c\ B\,\mathrm{d}r}{V^2(\theta, r)\ 2\,\pi\,r\,\mathrm{d}r} \tag{10}$$

where $V(\theta, r)$ is the free stream velocity at the position (θ, r).

The induced velocity is then derived as

$$u_{\mathrm{in}}(r, \theta) = V(\theta, r)\ a(r, \theta) \tag{11}$$

and $a(\theta, r)$ is derived from the equation

$$C_{\mathrm{T}}(\theta, r) = 4\,a(\theta, r)\ [1 - a(\theta, r)] \tag{12}$$

Wind Energ. 2012; **15**:63–81 © 2011 John Wiley & Sons, Ltd.
DOI: 10.1002/we

6.2. Discussion of implementation aspects

Three principal implementation methods of the BEM (BEM1, BEM2 and BEM3) have been illustrated above, representing the basic approach in the codes FLEX5, HAWC2 and GAST. However, for the use of the BEM model in an aeroelastic code where the induction has to be computed in combination with turbulence in the atmospheric inflow, for meandering wakes, for control actions of the turbine and for yawed operation, the induction computation must be thoroughly integrated with the submodels for the above conditions such as the engineering model for dynamic inflow (dynamic induction) and yawed flow. In particular, the dynamic inflow modeling has to be considered carefully with respect to the different BEM implementation methods. Hansen *et al.*[26] illustrates that because the time constant in the dynamic inflow model typically is several times bigger than the time for one rotor revolution, the dynamic inflow model will almost average out the azimuthal variation of the induction that will occur if the full unsteady BEM3 version is used.

In the HAWC2 code, this problem is overcome by computing at each time step the induction in a number of fixed points in space distributed over the rotor disk.[13,29] The instantaneous rotor loading is interpolated to these points where the unsteady induction is computed and the dynamic inflow model applied. Finally, at each time step, the induction on the blades are interpolated from the updated induction in the fixed points.

Another option is to apply the dynamic inflow filter to the mean of the unsteady induction from the three blades or at least the filter with the biggest time constant if more than one time constant is used as in the common procedure in dynamic inflow models.[30,31]

Finally, an option is to combine the BEM model with a near wake model[32] to compute the unsteady induction from the near part of the trailed vorticity of the individual blade. Again, the biggest time constant could be applied on the mean induction, and the near wake dynamic induction is modeled directly with the near wake model.[31]

6.3. Results for different implementations of BEM

The different BEM implementations briefly described above were tested in the same aeroelastic code, HAWC2, to obtain a comparison not influenced by a small difference between different codes. Further, it was also investigated what influence a typically used dynamic stall model, the Beddoes–Leishman model, has on the induction for sheared inflow. The specific version of the applied Beddoes–Leishman model was described by Hansen *et al.*[33]

The induction for the three BEM implementations is shown in Figure16, and further, the version BEM2 is shown without the dynamic stall model. The BEM1 implementation obviously gives the same induction for all four blade positions,

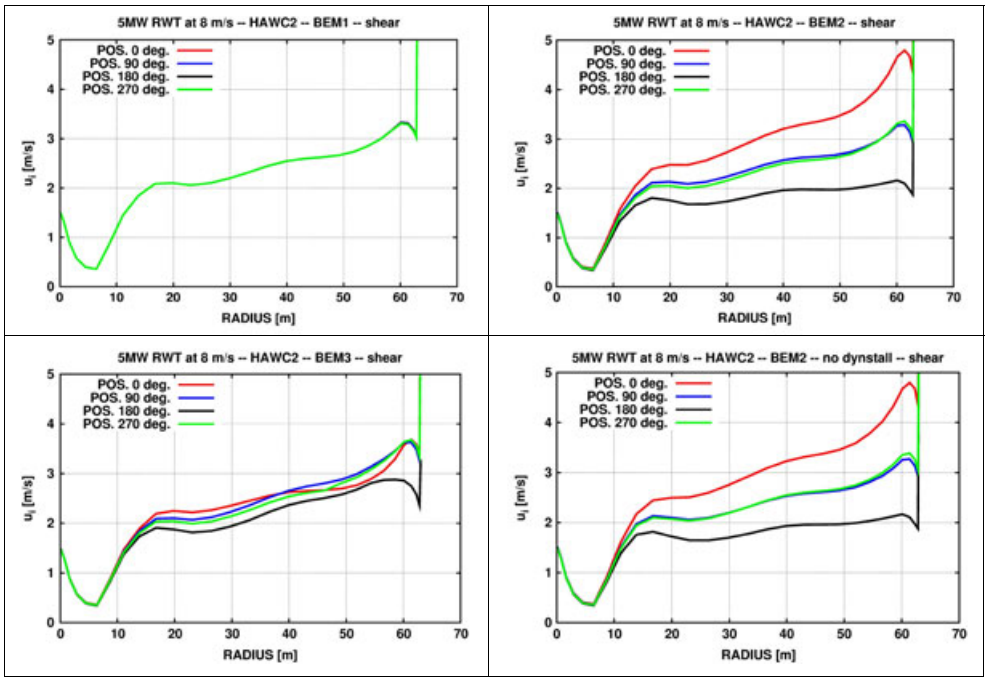


Figure 16. Induction at four blade positions for sheared inflow computed with different implementations of the BEM model. Additionally, the BEM2 was tested with and without a dynamic stall model.

whereas the BEM2 implementation gives the biggest difference in induction from vertical upward to vertical downward. The maximum difference in induction computed by BEM3 for the four blade positions is around 0.5 m s^{-1}, which seems to be slightly smaller than what the advanced model results showed. Comparing the two right graphs in Figure 16, we can see that the small difference in induction for the two horizontal blade positions are caused by the dynamic stall model.

The integrated power and thrust from the simulation with the different BEM versions is shown in Table II, and it is clear from these results that, in particular, the power is sensitive to the specific BEM implementation. The implementation method BEM1, where the induction is constant within an annular element, computes only a marginal decrease in power, whereas BEM2 gives a reduction of 3.8%. Finally, the full local induction of the computation of induction, BEM3, gives a small reduction in power of 1.8%. It also appears from Table II that the dynamic stall model has almost no influence on power and thrust.

7. EFFECT OF THE GROUND

The GENUVP and the AWSM models were used to study the influence of the ground. Additionally, the AWSM code was run for two different tower heights.

7.1. Results

The influence of the ground is illustrated by the plots of velocity contours and the vortex particle position shown in Figure 17, computed with the GENUVP code. From these plots, it is clear that one major effect is that the considerable expansion of the flow through the rotor is limited in the case with ground, as seen on the left panels in Figure 17. The interaction with the ground is also seen to cause a speed-up of the flow between the ground and the wake flow.

Power and thrust for the simulated cases are summarized in Table III. Both codes compute an increase in power for the sheared flow case with ground compared with the uniform inflow case, although the percentage increase is somewhat different for the two codes. To see the effect of an even stronger interaction with the ground, we run the AWSM code for a tower height of 75 m, and from Table III, it is seen that the power now increases with 11.2% relative to the uniform inflow case. Also, the tendency for the decrease in power for the case with shear but without ground is the same for the two codes although the numbers are quite different (Table III).

To summarize, the two vortex codes show an increase in power for the combined case of shear and ground, whereas the ACL code shows a small decrease in power when the ground is inserted (Table I). However, for the further refinement and validation of the BEM type modeling of sheared inflow, it is desirable to be able to separate the influence of the shear and the ground effect. One way to overcome this is to consider a test case with a wake from an upstream turbine (e.g., a half wake situation) instead of the present test case with shear in the atmospheric boundary layer. Such a test case would have much less interaction with the ground.

8. CONCLUSION

Considerable shear in the inflow is a common operational condition for MW turbines. This can be either due to shear in the atmospheric boundary layer, particularly in stable conditions, or be due to partial wake condition from an upstream turbine. The uncertainty in simulating such inflow conditions with the engineering BEM model used in most common aeroelastic codes is considerable. This is due to the lack of a well-documented implementation procedure of the BEM model for sheared inflow.

Analysis of results from the simulations of the advanced flow models on a rotor in sheared inflow shows a clear variation of the induction along the blade for different blade azimuthal positions. This gives guidance to an implementation of the BEM model in a version where the induction will vary as a function of azimuth position within an annular stream tube by applying the BEM equations locally on the rotor. This requires a careful integration with the dynamic inflow model in order

Table II. Power and thrust for the different BEM implementations.

BEM implementation method	Power (kW)	Thrust (kN)
BEM, uniform inflow	1928	391
BEM1, shear	1921	379
BEM2, shear	1855	380
BEM3, shear	1894	378
BEM2, shear, no dynamic stall model	1860	380

Wind Energ. 2012; **15**:63–81 © 2011 John Wiley & Sons, Ltd.
DOI: 10.1002/we

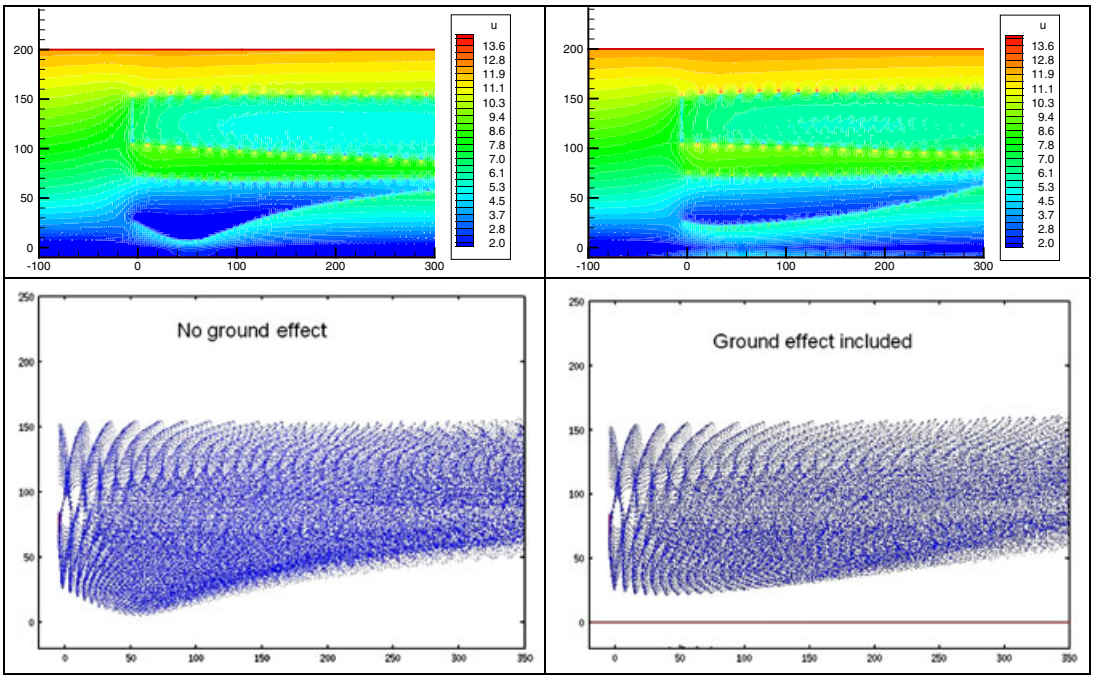


Figure 17. Computations of sheared flow and 90 m tower height with the GENUVP code without (left panels) and with (right panels) ground effect. The upper panels show the contour profiles of axial velocities, and in the lower panels, the vortex particles paths are shown.

Table III. Computation for different flow cases and two tower heights with the GENUVP and AWSM code, illustrating the ground effect on the rotor power and rotor thrust.

	Power (kW)		Thrust (kN)	
	GENUVP	AWSM	GENUVP	AWSM
No shear	1917	1953	363	382
Shear	1761	1942	341	373
% rel. to no shear	−8.1	−0.6	−6.1	−2.4
Shear and ground, 90 m tower height	1971	2078	360	386
% rel. to no shear	2.8	6.4	−0.8	1.0
Shear and ground, 75 m tower height	–	2188	–	390
% rel. to no shear		11.2		2.1

not to average out the time variations in induction over one rotor revolution. The present analysis shows that the specific implementation of the BEM model is important for the calculation of the rotor mean power and the rotor thrust.

The different flow mechanisms caused by the sheared inflow have been analysed on the basis of the advanced model results as well as dedicated engineering simulations. The starting point is a considerable higher power available in the sheared inflow compared with the uniform flow (6% in the present case). However, some flow mechanisms related to sheared inflow tend to decrease rotor power (e.g., variation of lift/drag ratio over rotor azimuth and variation of local C_T over the rotor disk), whereas others cause an increase. In particular, the interaction with the ground seems important for an increase in power.

ACKNOWLEDGEMENTS

The work presented has been carried out within the WP2 of the UpWind Project funded by the European Commission Union, call FP6-2004-Energy-3.

REFERENCES

1. Glauert H. Division L. Airplane propellers: II. The axial momentum theory. In *Aerodynamic Theory*, Vol. IV, Durand WF (ed.). Dover: New York, 1963.
2. Wilson RE, Lissaman PBS. *Applied Aerodynamics of Wind Power Machines*. Oregon State University: Newport, OR, 1974.
3. de Vries OM, AGARD Advisory Group for Aeroepace Research & Development AGARD-AG-243. Fluid Dynamic Aspects of Wind Energy Conversion, 1979; C4–C9.
4. Glauert H. Division L. Airplane propellers: XII. Miscellaneous airscrew problems. In *Aerodynamic Theory*, Vol. IV, Durand WF (ed.). Dover: New York, 1963.
5. Øye S. FLEX4 simulation of wind turbine dynamics. In *Proceedings of the 28th IEA Meeting of Experts Concerning State of the Art of Aeroelastic Codes for wind Turbine Calculations,* Technical University of Denmark, Lyngby, Pedersen BM (ed.), 11–12 April 1996; 129–135.
6. Bossanyi EA. *GH Bladed Theory Manual*. GH & Partners Ltd, 2003.
7. Larsen JT, Madsen HAa, Hansen AM, Thomsen K. Investigation of stability effects of an offshore turbine using the new aeroelastic code HAWC2. *Proceedings of the Copenhagen Offshore Wind*, 2005.
8. Larsen TJ (ed.). How 2 HAWC2, the user's manual. *Risø-r-1597(ver. 3–7)(en)*, Risø National Laboratory, 2009.
9. Jonkman JM, Buhl ML Jr. *FAST User's Guide. NREL/EL-500-29798*. National Renewable Energy Laboratory: Golden, CO, 2005.
10. Riziotis VA, Voutsinas SG. GAST: a general aerodynamic and structural prediction tool for wind turbines. *Proceedings of the EWEC'97*, Dublin, Ireland, 1997.
11. Madsen HAa, Fischer A. Wind shear and turbulence characteristics from inflow measurements on the rotating blade of a wind turbine rotor. *Paper presented at EWEC 2009 Scientific Proceedings*, Marseilles, France; 53–58.
12. Antoniou I, Wagner R, Pedersen SM, Paulsen US, Madsen HAa, Jørgensen HE, Thomsen K, Enevoldsen P, Thesbjerg L. Influence of wind characteristics on turbine performance (Invited Paper and Presentation). *Proceedings of the 2007 European Wind Energy Conference and Exhibition*, Milan, Italy, 7–10 May 2007. (EWEA, Brussels, 2007).
13. Madsen HAa, Mikkelsen R, Sørensen NN, Hansen MOL, Øye S, Johansen J. Influence of wind shear on rotor aerodynamics, power and loads. In *Research in Aeroelasticity EFP-2006*, Bak C (ed.), Risø-R-1611(EN), 2007; 101–116.
14. Madsen HAa, Vasilis R, Evangelos P, Hansen MOL, Snel H, Timmer N, Sørensen NN, Johansen J, McCann G. Short-comings in state of the art engineering aerodynamic and aeroelastic models by comparison to advanced models. *UPWIND Report Deliverable 2.2*, 7 May 2008.
15. Jonkmann J, Butterfield S, Musial W, Scott G. Definition of a 5-MW reference wind turbine for offshore system. *Development Technical Report NREL/TP-500-38060*, February 2009.
16. Michelsen JA. Basis3D—a platform for development of multiblock PDE solvers. *Technical Report AFM 92-05*, Technical University of Denmark, 1992.
17. Michelsen JA. Block structured multigrid solution of 2D and 3D elliptic PDE's. *Technical Report AFM 94-06*, Technical University of Denmark, 1994.
18. Sørensen NN. *General purpose flow solver applied to flow over hills*. Risø National Laboratory: Roskilde, Denmark, June 1995.
19. Sørensen JN, Shen WZ. Numerical modelling of wind turbine wakes. *Journal of Fluids Engineering* 2002; **124**(2): 393–399.
20. Voustinas SG. Vortex methods in aeronautics: how to make things work. *International Journal of Computational Fluid Dynamics* 2006; **20**: 3–18.
21. Van Garrel A. Development of a wind turbine aerodynamics simulation module. *ECN-C-03-079*, August 2003.
22. Grasso F. AWSM ground and wind shear effects in aerodynamic calculations. *ECN-E-10-016*, February 2010.
23. Grasso F. AWSM external field calculations. *ECN-X-09-043*, April 2009.
24. Zahle F, Sørensen NN. UpWind: Navier–Stokes rotor flow simulations with ground proximity and shear. *Paper presented at TORQUE 2010*, Heraklion, Crete, 28–30 June 2010.
25. Mikkelsen F, Sørensen JN, Troldborg N. Prescribed wind shear modelling with the actuator line technique. *Presented at EWEC, European Wind Energy Conference*, Milan, Italy, 2007.
26. Hansen OL, Mikkelsen RF, Øye S. Investigation the effect of extreme shear and yaw model using Actuator Line model. *Paper presented at TORQUE 2010*, Heraklion, Crete, 28–30 June 2010.

Wind Energ. 2012; **15**:63–81 © 2011 John Wiley & Sons, Ltd.
DOI: 10.1002/we

27. Ceyhan O, Bot ETG. Validation of the ECN Blade Optimization Tool BOT. *ECN-X-09-140*, Petten, The Netherlands, December 2009.
28. Troldborg N, Gaunaa M, Mikkel M. Actuator disc simulations of influence of wind shear on power production of wind turbines. *Paper presented at TORQUE*, Heraklion, Crete, 28.
29. Madsen HAa. Aerodynamic modelling in the aeroelastic codes HAWC and HAWC2. *IEA Joint Action Committee on Aerodynamics, Annex XI and 20. Aero Experts Meeting*, Pamplona, Spain, 25–26 May 2005.
30. Snel H, Schepers JG. Joint investigation of dynamic inflow effects and implementation of an engineering method. *ECN-C–94-107*, 1995.
31. Sørensen NN, Madsen HAa. Modelling of transient wind turbine loads during pitch motion. *Proceedings of the 2006 European Wind Energy Conference and Exhibition*, Athens, Greece, 27 February–2 March 2006. (European Wind Energy Association, Brussels, 2006).
32. Madsen HAa, Rasmussen F. A near wake model for trailing vorticity compared with the blade element momentum theory. *Wind Energy* 2004; **7**: 325–341.
33. Hansen MH, Gaunaa M, Madsen HAa. A Beddoes–Leishman type dynamic stall model in state-space and indicial formulations. *Risø-R-1354(EN)*, 2004.